General Disclaimer

One or more of the Following Statements may affect this Document

- This document has been reproduced from the best copy furnished by the organizational source. It is being released in the interest of making available as much information as possible.

- This document may contain data, which exceeds the sheet parameters. It was furnished in this condition by the organizational source and is the best copy available.

- This document may contain tone-on-tone or color graphs, charts and/or pictures, which have been reproduced in black and white.

- This document is paginated as submitted by the original source.

- Portions of this document are not fully legible due to the historical nature of some of the material. However, it is the best reproduction available from the original submission.

Produced by the NASA Center for Aerospace Information (CASI)

NASA Technical Memorandum 78570

(NASA-TM-78570) AN IMPLICIT ALGORITHM FOR THE CONSERVATIVE, TRANSONIC FULL-POTENTIAL EQUATION WITH EFFECTIVE ROTATED DIFFERENCING (NASA) 37 p HC A03/MF A01 CSCL 01A

N79-23909

Unclas
G3/02 20904

An Implicit Algorithm for the Conservative, Transonic Full-Potential Equation With Effective Rotated Differencing

Terry L. Holst and John Albert

1979
RECEIVED
NASA STI FACILITY
ACCESS DEPT.

April 1979

NASA
National Aeronautics and
Space Administration

NASA Technical Memorandum 78570

An Implicit Algorithm for the Conservative, Transonic Full-Potential Equation With Effective Rotated Differencing

Terry L. Holst, Ames Research Center, Moffett Field, California
John Albert, University of Santa Clara, Santa Clara, California

NASA
National Aeronautics and
Space Administration

Ames Research Center
Moffett Field, California 94035

AN IMPLICIT ALGORITHM FOR THE CONSERVATIVE, TRANSONIC FULL POTENTIAL EQUATION WITH EFFECTIVE ROTATED DIFFERENCING

Terry L. Holst

Ames Research Center

and

John Albert*

University of Santa Clara

SUMMARY

A new differencing scheme for the conservative full potential equation which effectively simulates rotated differencing is presented. The scheme is implemented by an appropriate upwind bias of the density coefficient along both coordinate directions. A fast, fully implicit, approximate factorization iteration scheme is then used to solve the resulting difference equations. Solutions for a number of traditionally difficult transonic airfoil test cases are presented.

I. INTRODUCTION

In reference 1, a new implicit approximate factorization algorithm (AF2) was presented. This algorithm has been applied to the solution of the transonic small-disturbance equation (ref. 2) and the conservative full potential equation (refs. 3 and 4). In both cases, significant improvements in convergence speed have been realized over standard successive line overrelaxation (SLOR) algorithms. Stability in the full potential formulations for supersonic regions of flow has been achieved by the addition of an artificial viscosity term similar to that introduced in reference 5. However, in the present formulation the addition of the artificial viscosity term has been achieved by an upwind bias of the density coefficient. This strategy greatly simplifies the solution procedure and effectively allows the simple two- and three-banded matrix form of the AF scheme to be retained over the entire flow field, even in regions of supersonic flow. Other researchers (refs. 5-8) have used similar steady-state differencing procedures in a wide variety of problems to further substantiate this approach as being both reliable and flexible.

The use of a numerical transformation to establish an arbitrary finite-difference mesh was introduced as an aspect of the present full potential

---

*Supported under NASA-Ames University Consortium Joint Research Interchange NCA2-OR685-803, currently graduate student, Dept. of Mathematics, University of Chicago, Chicago, Ill. 60637.

algorithm in reference 4. This grid generation technique was developed in reference 9 and has been extensively used for many applications (refs. 10 and 11). The basic transformation $(x,y \rightarrow \xi,\eta)$ is illustrated in figure 1. With this approach, body-fitted finite-difference meshes for arbitrary airfoil geometries can be routinely and efficiently generated. Extension of this procedure to more complicated geometries including three-dimensional problems is also possible.

In reference 4, the density coefficient was upwinded along only the wrap-around direction (ξ coordinate, see fig. 1) and not in the η-coordinate direction. Upwinding the density coefficient along only one coordinate direction does not in every case allow the numerical domain of dependence to fully accommodate the physical domain of dependence. Hence, in certain cases (usually solutions with strong shock waves), convergence is difficult or impossible to achieve. The purpose of this investigation is to develop an effective form of "rotated" differencing which will allow the numerical domain of dependence to more nearly match the physical domain of dependence, and thereby, improve the reliability of the present algorithm.

The finite-difference scheme including the new rotated differencing is presented in the next section along with several helpful guidelines for improving the convergence speed of the AF2 algorithm. The last section contains a variety of computational results including several classically difficult test cases which subject the new differencing scheme to the extreme test.

The authors express their gratitude to Vladimir Drobot, University of Santa Clara, for his assistance during the course of this study.

II. THE FULL POTENTIAL EQUATION ALGORITHM

A. Governing Equations

The full potential equation written in strong conservation-law form is given by

$$(\rho\phi_x)_x + (\rho\phi_y)_y = 0 \tag{1a}$$

$$\rho = \left[1 - \frac{\gamma - 1}{\gamma + 1}\left(\phi_x^2 + \phi_y^2\right)\right]^{1/\gamma - 1} \tag{1b}$$

where the density (ρ) and velocity components (ϕ_x and ϕ_y) are nondimensionalized by the stagnation density (ρ_s) and the critical sound speed (a_*), respectively; x and y are Cartesian coordinates; and γ is the ratio of specific heats.

Equation (1) expresses mass conservation for flows that are isentropic and irrotational. The corresponding shock-jump conditions are valid

approximations to the Rankine-Hugoniot relations for many transonic flow applications. A comparison of the isentropic and Rankine-Hugoniot shock polars is given in reference 12.

Equation (1) is transformed from the physical domain (Cartesian coordinates) into a computational domain by using a general independent variable transformation. This general transformation, indicated by (see fig. 1)

$$\left.\begin{aligned} \xi &= \xi(x,y) \\ \eta &= \eta(x,y) \end{aligned}\right\} \tag{2}$$

maintains the strong conservation-law form of equation (1) as discussed in references 10 and 13-15. The full potential equation written in the computational domain (ξ-η coordinate system) is given by

$$\left(\frac{\rho U}{J}\right)_{\xi} + \left(\frac{\rho V}{J}\right)_{\eta} = 0 \tag{3a}$$

$$\rho = \left[1 - \frac{\gamma - 1}{\gamma + 1}\left(U\phi_{\xi} + V\phi_{\eta}\right)\right]^{1/\gamma - 1} \tag{3b}$$

where

$$\left.\begin{aligned} U &= A_1\phi_{\xi} + A_2\phi_{\eta} \\ V &= A_2\phi_{\xi} + A_3\phi_{\eta} \\ A_1 &= \xi_x{}^2 + \xi_y{}^2 \\ A_2 &= \xi_x\eta_x + \xi_y\eta_y \\ A_3 &= \eta_x{}^2 + \eta_y{}^2 \\ J &= \xi_x\eta_y - \xi_y\eta_x \end{aligned}\right\} \tag{4}$$

U and V are the contravariant velocity components along the ξ and η directions, respectively; A_1, A_2, and A_3 are metric quantities; and J is the Jacobian of the transformation.

The transformed full potential equation (eq. (3)) is only slightly more complicated than the original Cartesian form (eq. (1)) and offers several significant advantages. The main advantage is that boundaries associated with the physical domain are transformed to boundaries of the computational domain. This aspect is illustrated in figure 1, where the physical and computational domains for a typical transformation are shown. The inner airfoil boundary becomes the $\eta = \eta_{max}$ computational boundary. Note that no restrictions have been placed on the shape of the outer boundary. Arbitrarily shaped outer boundaries, including wind-tunnel walls, may be used.

B. Grid Generation

The grid generation algorithm used in the present study is an adaptation of the scheme introduced by Thompson, Thames, and Mastin (ref. 9) and has been discussed in detail in reference 4. Basically, this scheme uses numerically generated solutions of Laplace's equation (or in some cases Poisson's equation) to establish regular and smooth finite-difference meshes around arbitrary bodies. These equations are transformed to (and solved in) the computational domain (i.e., ξ and η are the independent variables and x and y are the dependent variables). A fast approximate factorization relaxation algorithm is used to solve these equations. Once values of x and y are known for each point in the mesh, the metric quantities of equation (4) are computed by standard finite-difference formulas. Further details about this procedure are found in reference 4.

C. Spatial Differencing

A second-order accurate finite-difference approximation to the full potential equation (eq. (3a)) is given by

$$\overleftarrow{\delta}_{\xi}\left(\frac{\rho U}{J}\right)_{i+1/2,j} + \overleftarrow{\delta}_{\eta}\left(\frac{\rho V}{J}\right)_{i,j+1/2} = 0 \tag{5a}$$

where

$$\begin{aligned} U_{i+1/2,j} = {} & A_{1_{i+1/2,j}}(\phi_{i+1,j} - \phi_{i,j}) \\ & + \frac{1}{4} A_{2_{i+1/2,j}}(\phi_{i+1,j+1} - \phi_{i+1,j-1} \\ & + \phi_{i,j+1} - \phi_{i,j-1}) \end{aligned} \tag{5b}$$

$$\begin{aligned} V_{i,j+1/2} = {} & \frac{1}{4} A_{2_{i,j+1/2}}(\phi_{i+1,j+1} - \phi_{i-1,j+1} \\ & + \phi_{i+1,j} - \phi_{i-1,j}) \\ & + A_{3_{i,j+1/2}}(\phi_{i,j+1} - \phi_{i,j}) \end{aligned} \tag{5c}$$

The quantities ρ, A_1, A_2, A_3, and J are all stored at integer points in the finite-difference mesh (i.e., at i,j). Values needed at half points (i.e., $i+1/2,j$ or $i,j+1/2$) are obtained by using simple averages. The operators,

$$\overleftarrow{\delta}_{\xi}(\ ) \quad \text{and} \quad \overleftarrow{\delta}_{\eta}(\ )$$

are first-order accurate backward difference operators in the ξ and η directions, respectively, and are defined by

$$\overleftarrow{\delta}_{\xi}( )_{i,j} = ( )_{i,j} - ( )_{i-1,j}$$

$$\overleftarrow{\delta}_{\eta}( )_{i,j} = ( )_{i,j} - ( )_{i,j-1}$$

The density calculation is performed in a straightforward manner by using equation (3b). Values of U, V, ϕ_{ξ}, and ϕ_{η} required for the density calculation are given by

$$\left.\begin{aligned} \phi_{\xi_{i,j}} &= \frac{1}{2}\left(\phi_{i+1,j} - \phi_{i-1,j}\right) \\ \phi_{\eta_{i,j}} &= \frac{1}{2}\left(\phi_{i,j+1} - \phi_{i,j-1}\right) \\ U_{i,j} &= \left(A_1\phi_{\xi} + A_2\phi_{\eta}\right)_{i,j} \\ V_{i,j} &= \left(A_2\phi_{\xi} + A_3\phi_{\eta}\right)_{i,j} \end{aligned}\right\} \tag{6}$$

Special formulas replace equations (5) and (6) at boundaries and are discussed in reference 4.

Equation (5) is a suitable finite-difference scheme for subsonic flow regions. However, for supersonic regions, a properly chosen artificial viscosity term must be added. For example, Jameson (ref. 5) adds the following viscosity term to the Cartesian form of the full potential equation:

$$-\Delta x(\nu\rho_x\phi_x)_x - \Delta y(\nu\rho_y|\phi_y|)_y \tag{7}$$

where $\nu = \max[0, 1 - (1/M^2)]$ (M is the local Mach number). Exact implementation of equation (7) in the present case involving the $\xi - \eta$ coordinate system is difficult. Approximate implementation was achieved in reference 4 by using an artificial viscosity of the following form

$$-\Delta\xi\left(\nu\rho_{\xi}\left|\frac{U}{J}\right|\right)_{\xi} \tag{8}$$

where the absolute value of the U-velocity component has been included as a consequence of the wraparound coordinate system. Equation (8) is a good approximation to the first term of equation (7) on the upper and lower surfaces of an airfoil where the general $\xi - \eta$ coordinate system is approximately Cartesian. This strategy has been very successful for cases in which the supersonic zones are relatively small (i.e., cases in which the leading and trailing edges are reasonably far removed from supersonic flow). However, for cases containing strong shock waves at the trailing edge or supersonic free streams, a more complete approximation to equation (7) is required. An obvious extension of equation (8) is given by

$$-\Delta\xi\left(\nu\rho_\xi\left|\frac{U}{J}\right|\right)_\xi - \Delta\eta\left(\nu\rho_\eta\left|\frac{V}{J}\right|\right)_\eta \tag{9}$$

As pointed out by Jameson (ref. 5), addition of equation (7) (with appropriate upwind differencing) to the centrally differenced full potential equation (Cartesian form) provides automatic upwind differencing of the streamwise terms in supersonic regions, thus including the full effect of rotated differencing. Use of equation (9) (with appropriate upwind differencing), therefore, closely approximates the effects of a rotated differencing scheme.

The complete finite-difference approximation to equation (3a) is given by

$$\overleftarrow{\delta}_\xi\left(\frac{\rho U}{J}\right)_{i+1/2,j} + \overleftarrow{\delta}_\eta\left(\frac{\rho V}{J}\right)_{i,j+1/2} - \overleftarrow{\delta}_\xi\left[\left(\frac{\nu U}{J}\right)_{i+1/2,j}\left(\rho_{i+1/2,j} - \rho_{i+k+1/2,j}\right)\right]$$
$$- \overleftarrow{\delta}_\eta\left[\left(\frac{\nu V}{J}\right)_{i,j+1/2}\left(\rho_{i,j+1/2} - \rho_{i,j+\ell+1/2}\right)\right] = 0 \tag{10}$$

where

$$k = \begin{cases} -1 & \text{when } U_{i+1/2,j} > 0 \\ 1 & \text{when } U_{i+1/2,j} < 0 \end{cases} \tag{11a}$$

$$\ell = \begin{cases} -1 & \text{when } V_{i,j+1/2} > 0 \\ 1 & \text{when } V_{i,j+1/2} < 0 \end{cases} \tag{11b}$$

In the artificial viscosity term, ρ_ξ is evaluated with a backward difference when $U_{i+1/2,j} > 0$ and with a forward difference when $U_{i+1/2,j} < 0$. Likewise, ρ_η is evaluated with a backward difference when $V_{i,j+1/2} > 0$ and with a forward difference when $V_{i,j+1/2} < 0$. This maintains an upwind influence in the differencing scheme for supersonic regions anywhere in the finite-difference mesh for any orientation of the velocity vector. The test on $U_{i+1/2,j}$ is determined by whether a grid point is in the upper or lower half of the airfoil flow field, thus simplifying the computational algorithm.

The scheme given by equations (10) and (11) is centrally differenced and second-order accurate in subsonic regions. In supersonic regions, the differencing is a combination of the second-order accurate central differencing used in subsonic regions and the first-order accurate upwind differencing resulting from the addition of artificial viscosity. As the flow becomes increasingly supersonic, the scheme is increasingly retarded in the upwind direction.

As shown in reference 3, equation (10) can be rearranged to give

$$\overleftarrow{\delta}_{\xi}\left[\tilde{\rho}_i\left(\frac{U}{J}\right)_{i+1/2,j}\right] + \overleftarrow{\delta}_{\eta}\left[\bar{\rho}_j\left(\frac{V}{J}\right)_{i,j+1/2}\right] = 0 \tag{12a}$$

where

$$\tilde{\rho}_i = [(1 - \nu)\rho]_{i+1/2,j} + \nu_{i+1/2,j}\rho_{i+k+1/2,j} \tag{12b}$$

$$\bar{\rho}_j = [(1 - \nu)\rho]_{i,j+1/2} + \nu_{i,j+1/2}\rho_{i,j+\ell+1/2} \tag{12c}$$

The addition of the artificial viscosity given by equation (9) is thus equivalent to retarding the density in equation (5a). Artificial viscosity is not added explicitly as in the Jameson procedure.

In the η direction near the airfoil boundary, a problem arises when the V-component of velocity is negative. The upwind biased density coefficient at i,NJ-1/2 ($\bar{\rho}_{NJ-1}$) requires the use of the density at i,NJ+1/2, which is outside the finite difference mesh (see eq. (12c)). A value of density at this location is extrapolated from interior values using

$$\rho_{i,NJ+1/2} = (15\rho_{i,NJ} - 10\rho_{i,NJ-1} + 3\rho_{i,NJ-2})/8$$

Other values of density exterior to the finite-difference mesh are not required since at the airfoil surface (j = NJ) the following boundary condition is applied:

$$\bar{\rho}_{NJ-1}\left(\frac{V}{J}\right)_{i,NJ-1/2} = -\bar{\rho}_{NJ}\left(\frac{V}{J}\right)_{i,NJ+1/2} \tag{13a}$$

This boundary condition applied in either subsonic or supersonic regions is first-order accurate. Another boundary condition, which is second-order accurate for subsonic flow and first-order accurate for supersonic flow, has been tried and can be expressed as

$$\left(\frac{\rho V}{J}\right)_{\eta}\Bigg|_{i,NJ} = \frac{8}{3}\bar{\rho}_{NJ-1/2}\left(\frac{V}{J}\right)_{i,NJ} - 3\bar{\rho}_{NJ-1}\left(\frac{V}{J}\right)_{i,NJ-1/2} + \frac{1}{3}\bar{\rho}_{NJ-2}\left(\frac{V}{J}\right)_{i,NJ-3/2} \tag{13b}$$

where the first term is zero because of the $V_{i,NJ} = 0$ boundary condition. Results using these two boundary conditions have been compared and displayed little or no difference.

Several variations of the spatial difference scheme given by equation (12) have been considered. These variations arise from different evaluations of the artificial viscosity coefficient ν and are presented as follows:

Version 1

If $M_{i+1/2,j} \geq 1$, then

$$\nu_{i+1/2,j} = (M^2_{i+1/2,j} - 1)C \tag{14a}$$

If $M_{i+1/2,j} < 1$, then

$$\nu_{i+1/2,j} = 0 \tag{14b}$$

Version 2

$$\nu_{i+1/2,j} = \begin{cases} \max[(M^2_{i,j} - 1)C, 0] \text{ for } U_{i+1/2,j} > 0 \\ \max[(M^2_{i+1,j} - 1)C, 0] \text{ for } U_{i+1/2,j} < 0 \end{cases} \tag{15}$$

where the standard supersonic form for ν (i.e., $\nu = 1 - 1/M^2$) has been multiplied by CM^2. The parameter C is a user-specified constant, usually between 1.0 and 2.0. Multiplication by this additional term is used to increase the amount of artificial viscosity and therefore, the amount of upwinding in the difference scheme. In addition, the value of ν is never allowed to exceed 1.0. This seems to improve the stability and in some cases improves the convergence rate. Expressions for $\nu_{i,j+1/2}$ are written similarly to those for $\nu_{i+1/2,j}$ and depend on $M_{i,j+1/2}$ and $V_{i,j+1/2}$.

In addition to the basic form of artificial viscosity already presented (see eq. (9)), another form was tested and is given by

$$-\Delta\xi\left(\nu\rho_\xi \frac{A_1}{J}\phi_\xi\right)_\xi - \Delta\eta\left(\nu\rho_\eta \frac{A_3}{J}\phi_\eta\right)_\eta \tag{16}$$

The complete finite-difference approximation to equation (3a) using this form of artificial viscosity is obtained similarly to equation (10) and will not be presented. The coefficient ν for this artificial viscosity form is evaluated similarly to the ν coefficient of version 2 (see eq. (15)). The only difference is that the sign test on $V_{i,j+1/2}$ is replaced by a sign test on $(\phi_\eta)_{i,j+1/2}$. This is desirable (for this case) because both the sign of ϕ_η and the density upwind direction should change at the same point to maintain consistency. This artificial viscosity form along with version 2 evaluation of ν will be referred to as version 3 in the section on computed results.

D. The AF2 Iteration Scheme

The AF2 fully implicit approximate factorization scheme used in the present study is discussed in reference 4. Implementation of the scheme is achieved by writing it in a two-step form given by

Step 1

$$\left[\alpha - \vec{\delta}_\eta \bar{\rho}_j^n \left(\frac{A_3}{J}\right)_{i,j-1/2}\right] f_{i,j}^n = \alpha\omega L\phi_{i,j}^n \tag{17}$$

Step 2

$$\left[\alpha\overleftarrow{\delta}_\eta \mp \alpha\beta\overrightleftarrows{\delta}_\xi - \overleftarrow{\delta}_\xi \tilde{\rho}_i^n \left(\frac{A_1}{J}\right)_{i+1/2,j} \vec{\delta}_\xi\right] C_{i,j}^n = f_{i,j}^n \tag{18}$$

where the n superscript is an iteration index, ω is a relaxation parameter (set equal to 1.8 for all cases), $L\phi_{i,j}^n$ is the nth iteration residual operator (defined by eq. (12a)), and $f_{i,j}^n$ is an intermediate result stored at each point in the finite-difference mesh. In step 1, the f array is obtained by solving a simple bidiagonal matrix equation for each ξ = constant line. The correction array ($C_{i,j}^n = \phi_{i,j}^{n+1} - \phi_{i,j}^n$) is then obtained in the second step from the f array by solving a tridiagonal matrix equation for each η = constant line. Note that with the AF2 scheme the η-direction difference approximation is split between the two steps. This generates a $\phi_{\eta t}$ type term, which is useful to the iteration scheme as timelike dissipation. (The iterative process is considered as an iteration in pseudotime. Thus, the time derivative is introduced by $(\ )^{n+1} - (\ )^n \sim (\ )_t$.) The split η term also places a sweep direction restriction on both steps, namely, outward (away from the airfoil) for the first step and inward (toward the airfoil) for the second step. No sweep restrictions are placed on either of the two sweeps due to flow direction.

A $\phi_{\xi t}$ type term has been added inside the brackets of step 2 (see eq. (18)), to provide time-dependent dissipation in the ξ direction. The parameter β is determined as follows

$$\beta_{i,j} = \begin{cases} \beta_{M>1} & \text{if } \begin{cases} M_{i-1,j} \geq 1 & \text{upper surface} \\ M_{i+1,j} \geq 1 & \text{lower surface} \end{cases} \\ \beta_{M<1} & \text{if } \begin{cases} M_{i-1,j} < 1 & \text{upper surface} \\ M_{i+1,j} < 1 & \text{lower surface} \end{cases} \end{cases} \tag{19}$$

where $\beta_{M<1}$ is fixed at a value of 0.3 and $\beta_{M>1}$ is a user specified constant which can be adjusted as needed. (The default value for $\beta_{M>1}$ is equal to 1.0, which is sufficient to stabilize most moderate strength shock-wave calculations.) The double arrow notation on the ξ-difference operator indicates that the difference is always upwind, which on the upper surface is a backward difference and on the lower surface is a forward difference. The sign is chosen in such a way that the addition of $\phi_{\xi t}$ increases the magnitude of the second sweep diagonal.

The quantity α appearing in equations (17) and (18) can be considered as Δt^{-1}. This direct analogy to time provides one strategy for obtaining

fast convergence, namely, advance time as fast as possible with large time steps (i.e., small values of α). As pointed out in reference 3, this is effective for attacking the low-frequency errors but not the high-frequency errors. The best overall approach is to use an α sequence containing several values of α. The small values are particularly effective for reducing the low-frequency errors, and the large values are particularly effective for reducing the high-frequency errors. A suitable α sequence with analytically estimated endpoints is given in reference 3.

An additional possibility for improving the convergence rate is to not only use an α sequence, but also vary the α sequence with spatial position. With such a strategy, the α sequence can be adjusted locally to accommodate any type of error, i.e., a relatively large residual would indicate a high-frequency error and the need for smaller alphas, and a relatively small residual would indicate low-frequency error and the need for larger alphas. To date, this strategy has not been implemented in any sophisticated manner. However, a simplified version has been tested which assumes that the highest frequency errors will be supported in the finest region of the finite-difference mesh (i.e., near the airfoil). In this region (specifically for the three η = constant coordinate lines nearest the airfoil), the lowest alphas (largest time steps) are never allowed to fall below a certain value. With this constraint, it was found that the lowest global values of alpha could be reduced by as much as a factor of five which resulted in a convergence rate improvement of roughly a factor of two.

Normally, flow-field, type-dependent differencing is used to achieve stability in transonic flow calculations. Incorporating these different operators into iteration procedures, such as the AF2 scheme presented here, would be cumbersome if not impossible. Using the upwind bias of the density coefficient, which is always evaluated at the nth iteration level, allows the simple two- and three-banded matrix form of the AF2 scheme to be retained over the entire flow field, even in regions of supersonic flow. In fact, use of upwinded density coefficients in any general iteration scheme could be used to remove the difficulties introduced by type-dependent differencing. The resulting general scheme would retain the same basic differencing (at the $n + 1$ iteration level) throughout the entire flow field, relying on the upwind bias of the density (at the nth iteration level) to provide the artificial viscosity in supersonic flow regions. This represents a significant simplification in the handling of supersonic flow regions for transonic flow calculations.

III. COMPUTED RESULTS

The new rotated differencing algorithm introduced in the previous section is evaluated in this section by presenting a range of numerically computed examples, including transonic and supersonic free-stream test cases. In all cases the numerically generated finite-difference mesh was converged until the maximum residual dropped by three orders of magnitude. For a typical mesh with 4470 grid points (149×30), this required approximately 30 to 40 iterations and about 5 sec of CPU time on the Ames 7600 computer. An example of a

numerically generated finite-difference mesh for the NACA 0012 airfoil is shown in figure 2.

A. Artificial Viscosity Variations

A series of calculations has been computed to determine the effect of the spatial differencing variations presented in the previous section. The test case chosen for this purpose is an NACA 0012 airfoil at a free-stream Mach number of 0.75 and 2° angle of attack. Systematic variations of the parameter C for all three artificial viscosity versions (see eqs. (14)-(16)), including both rotated (NDIF = 1) and nonrotated (NDIF = 0) forms, were investigated. (The nonrotated difference scheme simply has no η-direction artificial viscosity term. This causes the term $(\rho V/J)_\eta$ to remain centrally differenced in supersonic regions.) These solutions are typically represented by the pressure coefficient distributions shown in figures 3 and 4. As expected, cases involving larger amounts of artificial viscosity (i.e., larger values of C) produce slightly smaller lift coefficients and larger amounts of shock smearing. Use of the rotated differencing option (NDIF = 1) had a similar effect causing a slight amount of additional shock smearing. This trend was basically exhibited by each of the three differencing variations. Two of the schemes (versions 2 and 3) produced similar solutions for most of the cases. The version 1 solutions (see fig. 3) were somewhat different, displaying dispersive overshoots at the shock wave. Increasing the value of C reduces the size of the overshoot but does not entirely eliminate it. Some difficulty in maintaining stability as well as the normal convergence rate has been experienced with the version 1 scheme and is attributed to the existence of dispersion in these solutions.

The lack of an overshoot for the version 2 solutions (see fig. 4) can be explained as follows: The artificial viscosity coefficient $\nu_{i+1/2,j}$ as computed in the version 2 differencing scheme is actually evaluated at i,j (for $U_{i+1/2,j} > 0$) instead of at $i+1/2,j$. This effectively provides a substantial increase in the artificial viscosity at the shock wave, especially at the last supersonic point near the shock-wave center (because $\nu_{i,j}/\nu_{i+1/2,j} >> 1$ at this point), and usually a slight decrease in other supersonic regions (because $\nu_{i,j}/\nu_{i+1/2,j} < 1$). The effect of this substantial increase in artificial viscosity at the shock is to dramatically inhibit the formation of dispersive shock-wave overshoots. Since the version 1 differencing scheme does not have this property, shock-wave overshoots can be suppressed only by adding a large amount of artificial viscosity everywhere in the supersonic region.

Numerical experiments with other cases including several classically difficult cases, which will be presented in the next section, have been conducted with artificial viscosity versions 2 and 3. Although the differences were small, the version 2 differencing was chosen as superior. The main advantage was slightly faster and smoother convergence especially for supersonic free-stream cases. From this point on only artificial viscosity version 2 solutions will be presented.

B. Convergence Reliability

Three clasically difficult test cases have been investigated to help evaluate the convergence reliability of the present algorithm, especially the newly implemented rotated differencing option. These cases involve three different free-stream conditions for an NACA 0012 airfoil: (1) $M_\infty = 0.98$, $\alpha = 0°$, (2) $M_\infty = 0.95$, $\alpha = 4°$, and (3) $M_\infty = 1.15$, $\alpha = 0°$. Each case has an unusually large amount of supersonic flow and a rather unique shock-wave pattern. Classical relaxation schemes would probably experience either very slow convergence or instability with these cases.

Solutions with M_∞ approaching unity— The pressure coefficient distribution for the first case ($M_\infty = 0.98$, $\alpha = 0°$) is shown in figure 5. This case is nonlifting ($C_L = 0.0$ and $C_M = 0.0$) and has a large amount of wave drag ($C_D = 0.1038$). The airfoil is almost totally immersed in supersonic flow which begins at approximately 5% of chord and continues through an oblique shock wave at the trailing edge. A more complete description of the flow field is shown by the Mach number contour map displayed in figure 6. Existence of a rather unique double shock-wave structure, sometimes referred to as a "fishtail shock," is clearly evident. Relatively weak oblique shocks emanate from the trailing edge and merge with a normal shock downstream of the airfoil. The triangular region between the oblique and normal shocks has a nearly constant supersonic Mach number (approximately equal to 1.1). This shock-wave pattern is characteristic of solutions with free-stream Mach numbers near unity. It has been observed experimentally as well as computationally and is generally considered to be the correct qualitative solution. For instance, a fishtail shock solution, for a 10% circular arc airfoil at $M_\infty = 0.98$ and zero degrees angle of attack, was presented in reference 6. This calculation was a solution to the conservative full potential equation using a Cartesian mesh and small-disturbance boundary conditions. Because the flow was essentially aligned with the finite-difference mesh, "rotated differencing" was not necessary. However, with the present wraparound coordinate system, rotated differencing is essential for maintaining the stability of difficult cases such as the present fishtail shock solution. For example, in the supersonic triangle between the oblique and normal shocks (see fig. 6), the ξ direction is nearly normal to the direction of flow. This makes the ξ-direction artificial viscosity term ineffective in achieving an upwind influence. The upwind bias of the density along the η coordinate (which is achieved by a forward difference of ρ_η in the η-direction artificial viscosity term) provides the necessary upwind influence to stabilize the calculation.

Another very important ingredient for maintaining stable convergence is having the proper amount of timelike dissipation ($\phi_{\eta t}$ and $\phi_{\xi t}$). (This fact concerning AF schemes was first mentioned to the authors by J. South, NASA Langley.) A fixed amount of $\phi_{\eta t}$ is automatically added to the iterative process by the construction of the present AF2 algorithm. Likewise, the amount of $\phi_{\xi t}$ added in subsonic regions is also fixed ($\beta_{M<1} = 0.3$, see eq. (19)). The amount of $\phi_{\xi t}$ added in supersonic regions is controlled by a user-specified constant ($\beta_{M>1}$) which can be adjusted as needed. For the fishtail shock calculation just presented, the $\beta_{M>1}$ parameter was equal to five. Smaller values produced instabilities for this calculation.

As pointed out in reference 16, nonconservative full potential equation solutions with the free-stream Mach number approaching unity are characterized by strong oblique shock waves at the trailing edge followed by subsonic flow. The fishtail shock structure for these cases is not predicted. Conservative vs nonconservative differencing was the subject of discussion in reference 17 where similar differences for the transonic small-disturbance equation were reported. It is generally understood that these differences are the result of effective mass creation at shock waves for the nonconservative differencing schemes. Therefore, to obtain the proper mass balance and the correspondingly correct solution (to either the full potential or transonic small-disturbance potential equation), conservative differencing is required.

The pressure coefficient distribution for the second case (also involving a free-stream Mach number near unity ($M_\infty = 0.95$)) is shown in figure 7. This case is at an angle of attack of 4° and therefore produces lift ($C_L = 0.43$). The airfoil is again almost completely immersed in supersonic flow, which begins at about 5% of chord (upper surface) and continues through oblique shocks at the trailing edge. A more complete description of the flow field is shown by the Mach number contour map displayed in figure 8. The oblique shock emanating from the trailing edge upper surface has been strengthened by the addition of circulation while the oblique shock emanating from the trailing edge lower surface has weakened and is almost nonexistent. The normal shock above the airfoil is much stronger than the normal shock below the airfoil. Except for these changes, the basic structure of the fishtail shock pattern is the same as for the first case.

This is the first time in transonic flow computations that calculations such as those of the last two cases have been computed using an exact airfoil mapping. Without the newly developed rotated difference scheme these calculations would have been unstable. The difficulty of these cases demonstrates the reliability of the present transonic flow solution procedure.

Supersonic free-stream solutions— The pressure coefficient distribution for the last case ($M_\infty = 1.15$, $\alpha = 0°$) is shown in figure 9. This case like the first is nonlifting and has a large amount of wave drag ($C_D = 0.931$). The decrease in wave drag for this case relative to the first fits in well with the established C_D vs M trend. An oscillation in the pressure distribution at the trailing edge is exhibited for this case and is attributed to the interaction of the shock wave and the mapping singularity at the airfoil trailing edge. A more complete description of the entire flow field is shown by the Mach number contour map displayed in figure 10. A detached bow shock wave, characteristic of supersonic free streams, exists just upstream of the airfoil. Weak oblique shocks emanate from both the upper and lower surfaces at the airfoil trailing edge. The flow is supersonic at approximately 85% of all grid points in the flow field. The region of flow just downstream of the normal part of the bow shock and in the vicinity of the leading edge stagnation point is the only subsonic region. Thus, the finite-difference scheme over almost the entire flow field is first-order accurate.

Some difficulties were experienced with this calculation and are attributed to the use of standard subsonic boundary conditions on the outer boundary

(i.e., explicit specification of the free-stream solution). For instance, unstable results were obtained with the standard mesh. To stabilize this calculation the outer boundary had to be moved to a radius of 12 chords away from the airfoil instead of the usual 6 chords. In addition, the remesh option, which provides special grid point clustering at the airfoil (described in ref. 4), had to be used. Because supersonic free-stream cases are not of primary importance in the present study, no attempts have been made to stabilize this calculation on the standard mesh with a more appropriate supersonic outer boundary condition.

C. Convergence Speed

In the last section several classically difficult test cases have been presented in an attempt to establish the high level of reliability associated with the present new algorithm. Virtually any airfoil problem in the transonic range (i.e., subsonic free stream) is deemed solvable by the present technique. In this section the convergence rate of these solutions is examined. This topic was the subject of discussion in reference 4, where only moderately difficult cases were considered. An example of a particularly rapid convergence for an "easy" calculation is shown in figures 11 and 12. (The residual history for this calculation is given in ref. 4.) This calculation is subcritical ($M_\infty = 0.72$) and nonlifting ($\alpha = 0°$, NACA 0012). The pressure coefficient distributions after 9 and 15 iterations, with only every other point plotted for clarity, are compared with the solidly converged solution in figures 11 and 12, respectively. The solution trend is established after only 9 iterations, and plottable accuracy is established after only 15 iterations. The latter solution corresponds to a reduction in the maximum residual of about one and a half orders of magnitude and represents only about 2 sec of computer time. The convergence speed exhibited in this calculation represents the ultimate speed achievable with the present algorithm.

Of course, this type of convergence is not obtained in most cases. Both the existence of lift and supersonic regions of flow slow down convergence. An example of this is the convergence rate of the first case considered, i.e., an NACA 0012 airfoil, $M_\infty = 0.75$, and $\alpha = 2°$ (see section III.A). Convergence histories for this case are displayed in figure 13. The lift coefficient (C_L), number of supersonic points (NSP), and maximum residual ($|R|_{max}$), normalized to 1.0 for the first iteration, are all plotted vs iteration number (n). These curves, as well as all convergence history curves presented in this section, are constructed by plotting the appropriate quantity after every eighth iteration. The convergence rate in all cases has been approximately optimized by a trial and error process. Both NSP and C_L climb rapidly and reach 1% of their final values within 48 iterations. The lift coefficient overshoots slightly, which is characteristic of both C_L and NSP for many calculations. The flow field is essentially converged at this point even though the maximum residual has dropped by less than an order of magnitude.

Establishment of crude convergence for such a small reduction in the maximum residual is a characteristic behavior of many calculations using the present algorithm, especially for cases involving a large amount of supersonic

flow. For example, convergence history curves for the first two cases discussed in section III.B (fishtail shock cases) are presented in figures 14 and 15. The maximum residual in each case does not even start to drop until after the solutions are approximately converged. During the initial phase of convergence in which the residual does not drop, the shock sonic line's position is rapidly being adjusted. This excites high-frequency errors, and therefore, keeps the residual artificially high, even though the error is being reduced. The convergence history displayed in figure 14 indicates convergence in approximately 80 iterations, which is signified by the constant value of NSP. At this point the residual starts dropping exponentially, taking approximately 220 iterations to reach a six-order-of-magnitude reduction. The convergence history displayed in figure 15 indicates convergence in approximately 100 iterations, and is signified by constant values of both NSP and C_L. Shortly after this point the residual starts dropping exponentially, taking approximately 300 iterations to reach a six-order-of-magnitude reduction in maximum residual. The degradation in convergence speed of the latter case is associated with the addition of lift into the problem, and more specifically, by the approximate technique for updating the circulation in the vortex solution (e.g., see ref. 4). For larger amounts of lift the convergence rate will be even slower.

The last convergence history curve presented in figure 16 is associated with the last test case discussed in section III.B (NACA 0012, $M_\infty = 1.15$, $\alpha = 0°$). Because for this case all grid points in the flow field are initially supersonic, the value of the NSP parameter decreases (instead of increasing) to the correct value as the solution converges. This solution is essentially converged in 100 iterations. The maximum residual again hesitates in the initial phase of convergence and then drops exponentially, taking approximately 330 iterations to reach a six-order-of-magnitude reduction.

IV. CONCLUSIONS

A fast, implicit algorithm for solving the conservative full potential equation with effective rotated differencing has been presented. The rotated differencing is simply achieved by an upwind evaluation of the density coefficient along both coordinate directions. This provides an effective upwind difference of the streamwise terms for any orientation of the velocity vector (i.e., rotated differencing), and, thereby, greatly enhances the reliability of the present algorithm. Use of the newly developed rotated differencing scheme has been instrumental in computing a number of classically difficult test cases including several cases with "fishtail" shock-wave patterns and a case with a detached bow shock wave. This represents the first time such calculations have been computed using the conservative full potential equation with an exact airfoil mapping.

Results indicate that even for the classically difficult test cases presented herein, the solution convergence rate is maintained at an exceptionally high level, which is indicative of the present fully implicit approximate factorization (AF2) algorithm. A characteristic of the AF2 convergence history

for many cases containing a large amount of supersonic flow (i.e., strong shock waves), is that the solution is essentially converged before the maximum residual even begins to drop. This indicates that the high-frequency error content of the solution does not decay until the solution is essentially converged. Because of this feature, the need for a different convergence criteria, other than a specified reduction in the maximum residual, is indicated.

REFERENCES

1. Ballhaus, W. F.; and Steger, J. L.: Implicit Approximate Factorization Schemes for the Low-Frequency Transonic Equation. NASA TM X-73,082, 1975.

2. Ballhaus, W. F.; Jameson, A.; and Albert, J.: Implicit Approximate Factorization Schemes for the Efficient Solution of Steady Transonic Flow Problems. AIAA J., vol. 16, no. 6, 1978, pp. 573-579.

3. Holst, T. L.; and Ballhaus, W. F.: Fast Conservative Schemes for the Full Potential Equation Applied to Transonic Flows. NASA TM-78469, 1978. (Also AIAA J., Feb. 1979.)

4. Holst, T. L.: An Implicit Algorithm for the Conservative, Transonic Full Potential Equation Using an Arbitrary Mesh. AIAA Paper 78-1113, July 1978.

5. Jameson, A.: Transonic Potential Flow Calculations Using Conservative Form. AIAA Second Computational Fluid Dynamics Conference Proceedings, June 1975, pp. 148-155.

6. Hafez, M. M.; Murman, E. M.; and South, J. C.: Artificial Compressibility Methods for Numerical Solution of Transonic Full Potential Equation. AIAA Paper 78-1148, July 1978.

7. Eberle, A.: A Finite Volume Method for Calculating Transonic Potential Flow Around Wings from the Pressure Minimum Integral. Technical Translation. NASA TM-75,324, 1978.

8. Eberle, A.: Transonic Potential Flow Computations by Finite Elements: Airfoil and Wing Analysis, Airfoil Optimization. Lecture held at the DGLR/GARTEUR 6 Symposium, Transonic Configurations, Bad Harzburg, Germany, June 1978.

9. Thompson, J. F.; Thames, F. C.; and Mastin, C. M.: Automatic Numerical Generation of Body-Fitted Curvilinear Coordinate System for Field Containing Any Number of Arbitrary Two-Dimensional Bodies. J. of Comp. Physics, vol. 15, 1974, pp. 299-319.

10. Steger, J. L.: Implicit Finite Difference Simulation of Flow About Arbitrary Geometrics with Application to Airfoils. AIAA Paper 77-665, June 1977.

11. Hodge, J. K.; and Stone, A. L.: Numerical Solution for Airfoils Near Stall in Optimized Boundary-Fitted Curvilinear Coordinates. AIAA Paper 78-284, Jan. 1978.

12. Steger, J. L.; and Baldwin, B. S.: Shock Waves and Drag in the Numerical Calculation of Isentropic Transonic Flow. NASA TN D-6997, 1972.

13. Lapidus, A.: A Detached Shock Calculation by Second-Order Finite Differences. J. Comp. Physics, vol. 2, 1967, pp. 154-177.

14. Viviand, H.: Conservative Forms of Gas Dynamic Equations. La Recherche Aerospatiale, No. 1, Jan.-Feb. 1974, pp. 65-68.

15. Vinokur, M.: Conservative Equations of Gas Dynamics in Curvilinear Coordinate Systems. J. Comp. Physics, vol. 14, Feb. 1974, pp. 105-125.

16. Jameson, A.: Iterative Solution of Transonic Flows over Airfoils and Wings, Including Flows at Mach 1. Communications on Pure and Applied Math., vol. 27, 1974, pp. 283-309.

17. Newman, P. A.; and South, J. C.: Conservative Versus Nonconservative Differencing: Transonic Streamline Shape Effects. NASA TM X-72,827, 1976.

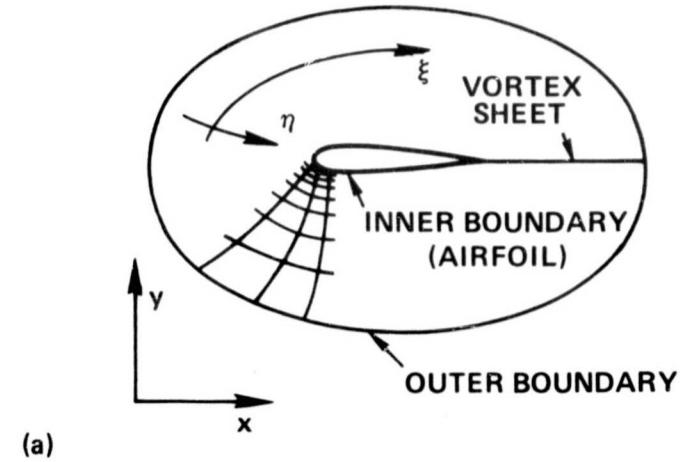

(a)

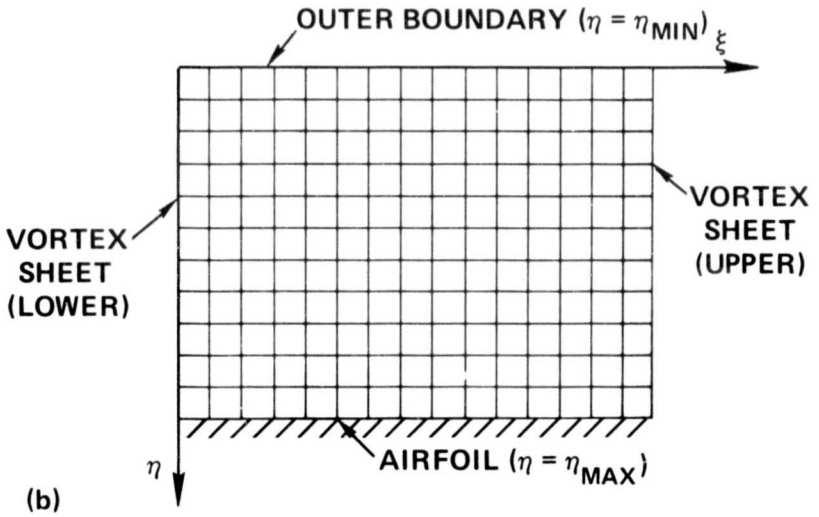

(b)

Figure 1.- Numerically generated transformation, $(x,y) \rightarrow (\xi,\eta)$.

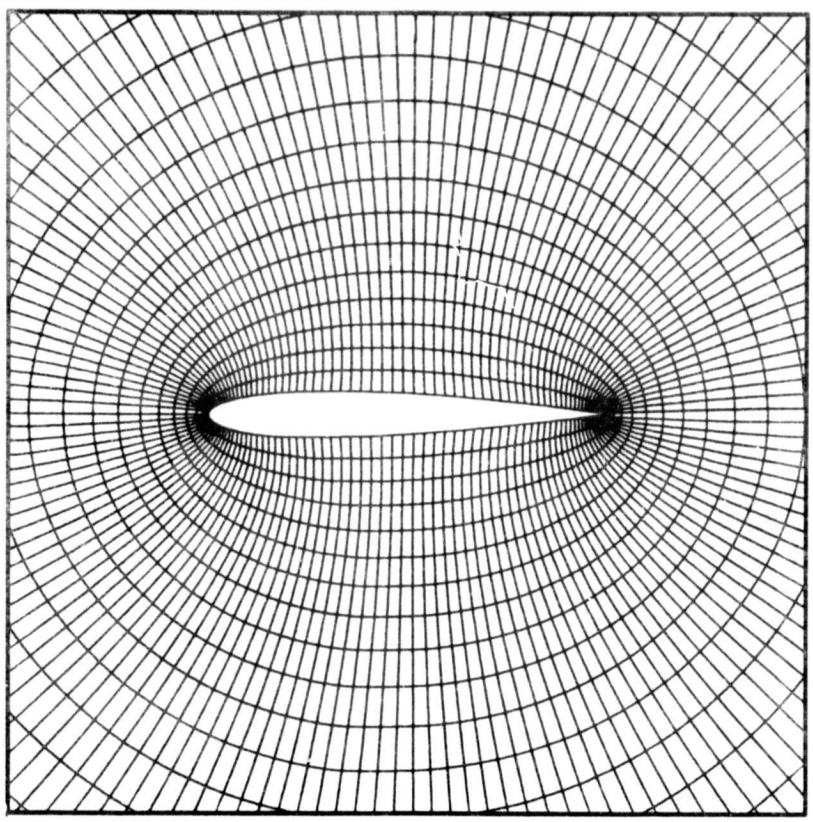

Figure 2.- Detail of a typical finite-difference mesh (NACA 0012 airfoil).

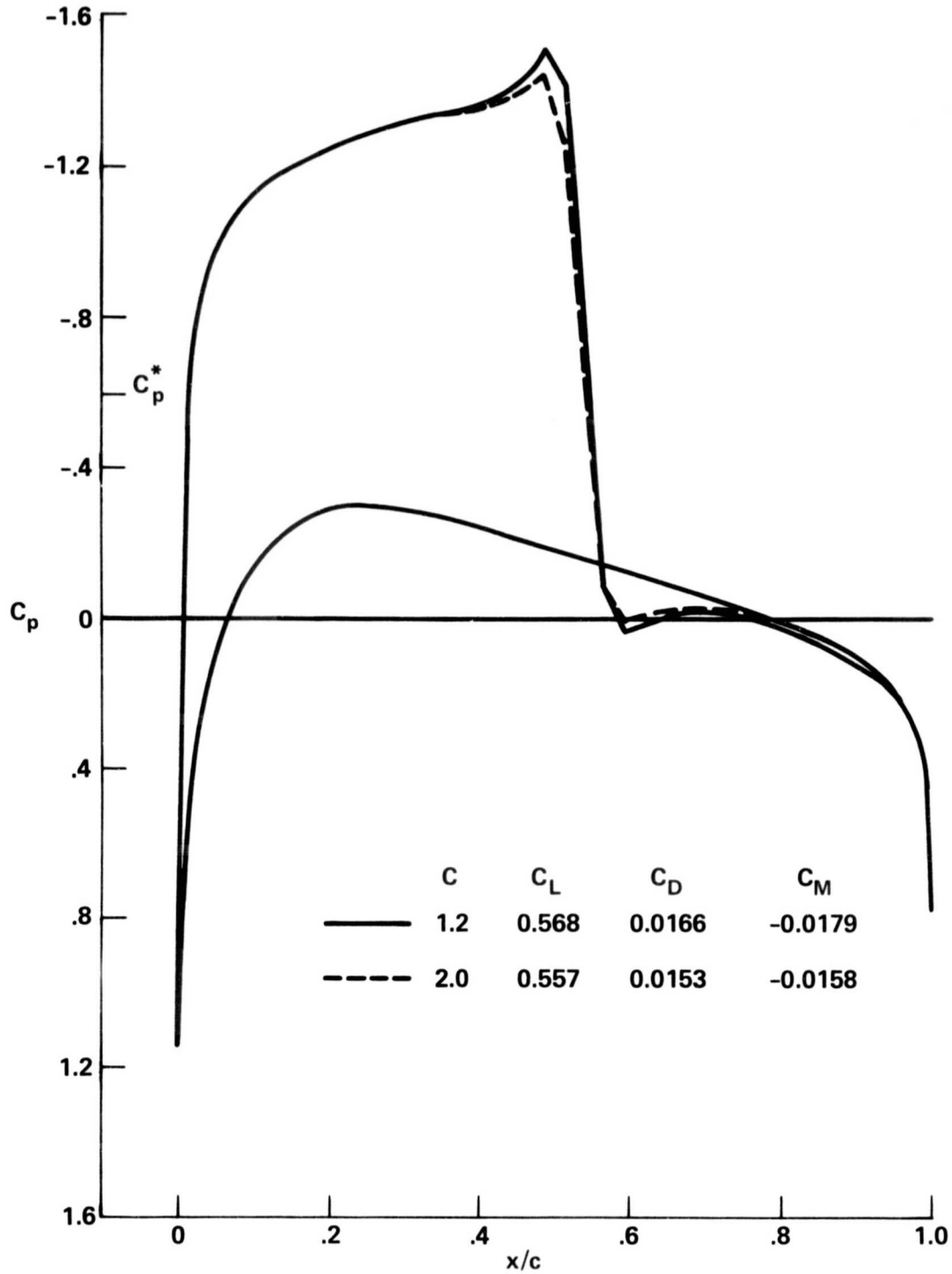

Figure 3.- Pressure coefficient distribution, artificial viscosity version 1, NACA 0012 airfoil, $M_\infty = 0.75$, $\alpha = 2°$.

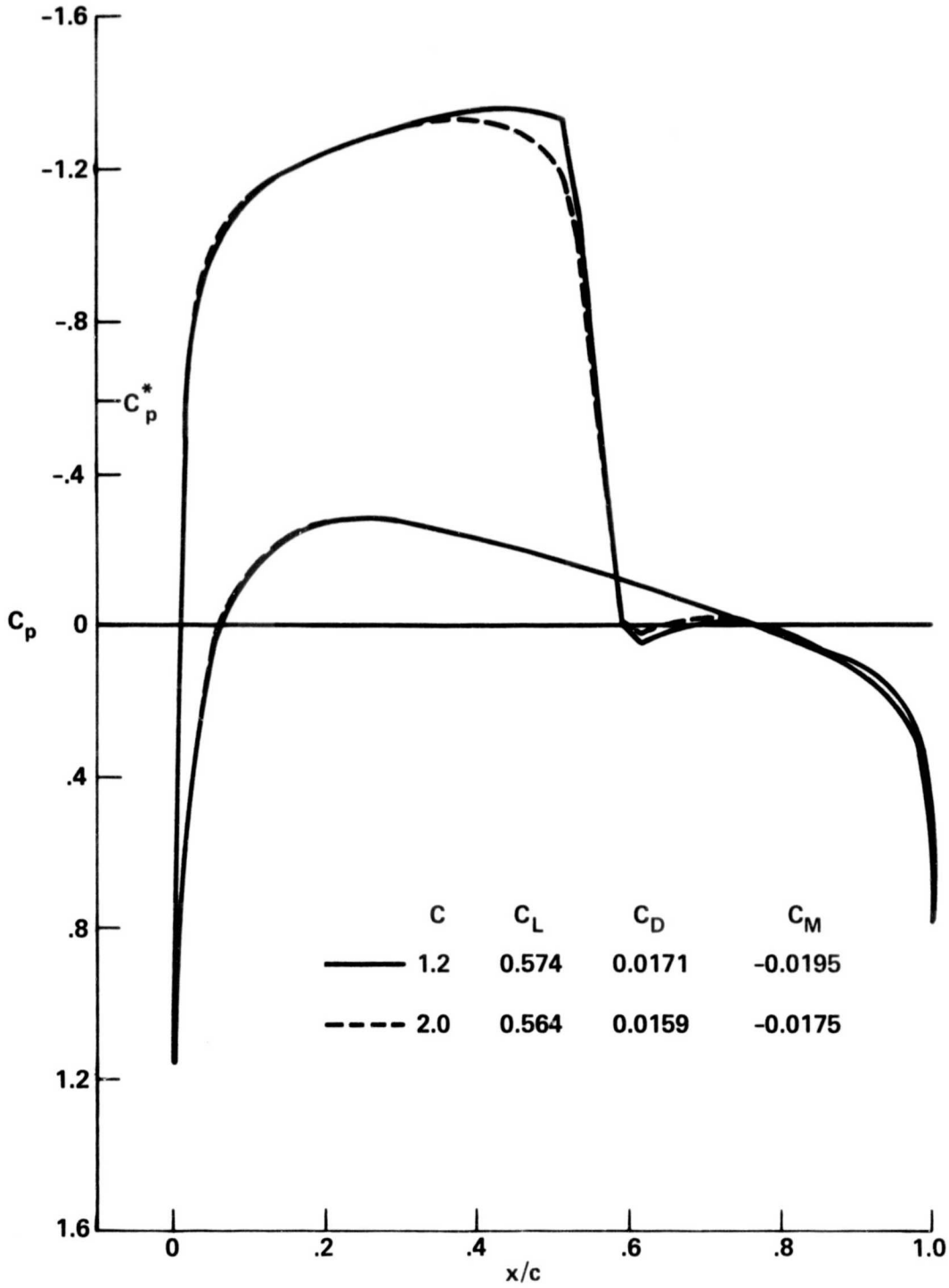

Figure 4.- Pressure coefficient distribution, artificial viscosity version 2, NASA 0012 airfoil, $M_\infty = 0.75$, $\alpha = 2°$.

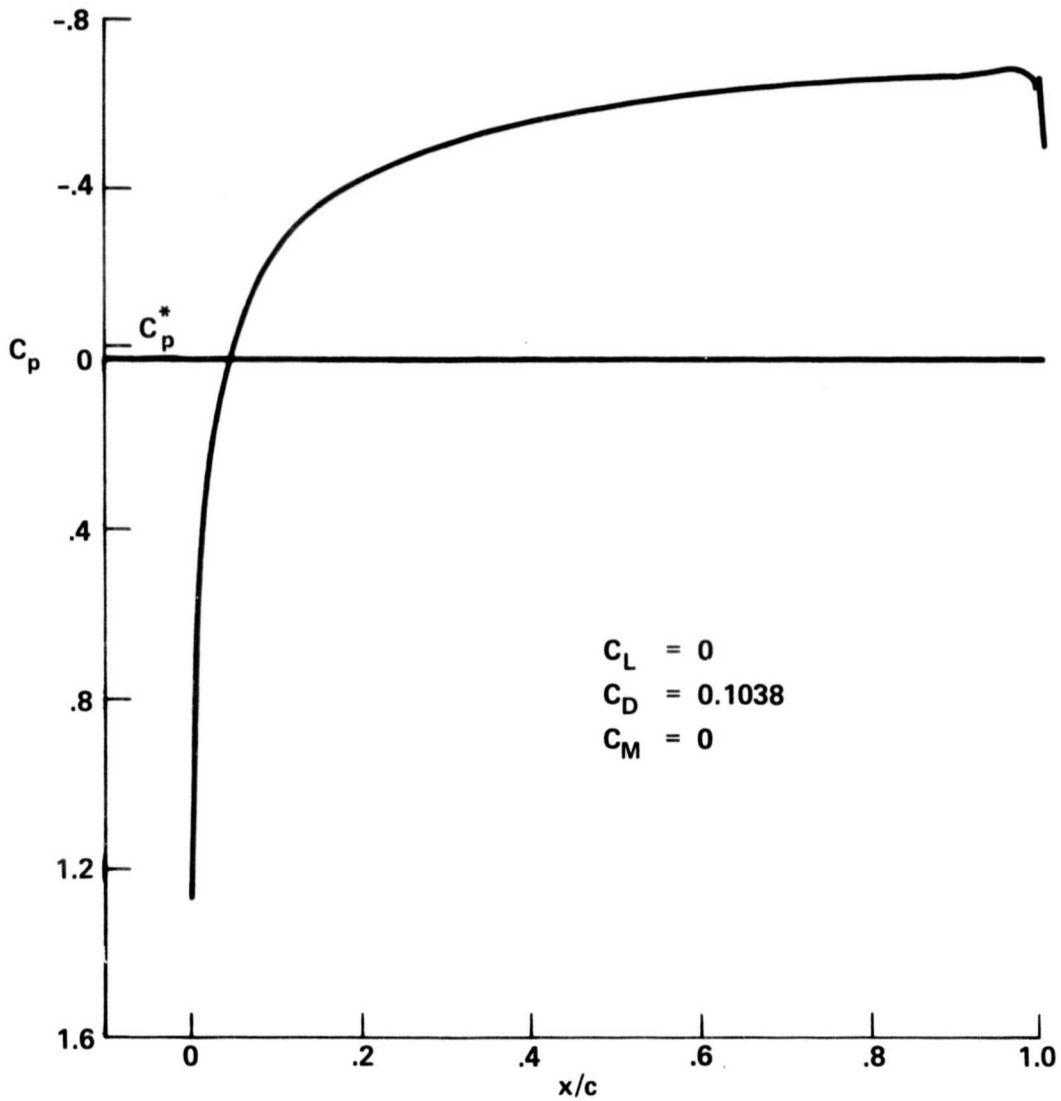

Figure 5.- Pressure coefficient distribution, NACA 0012 airfoil, $M_\infty = 0.98$, $\alpha = 0°$.

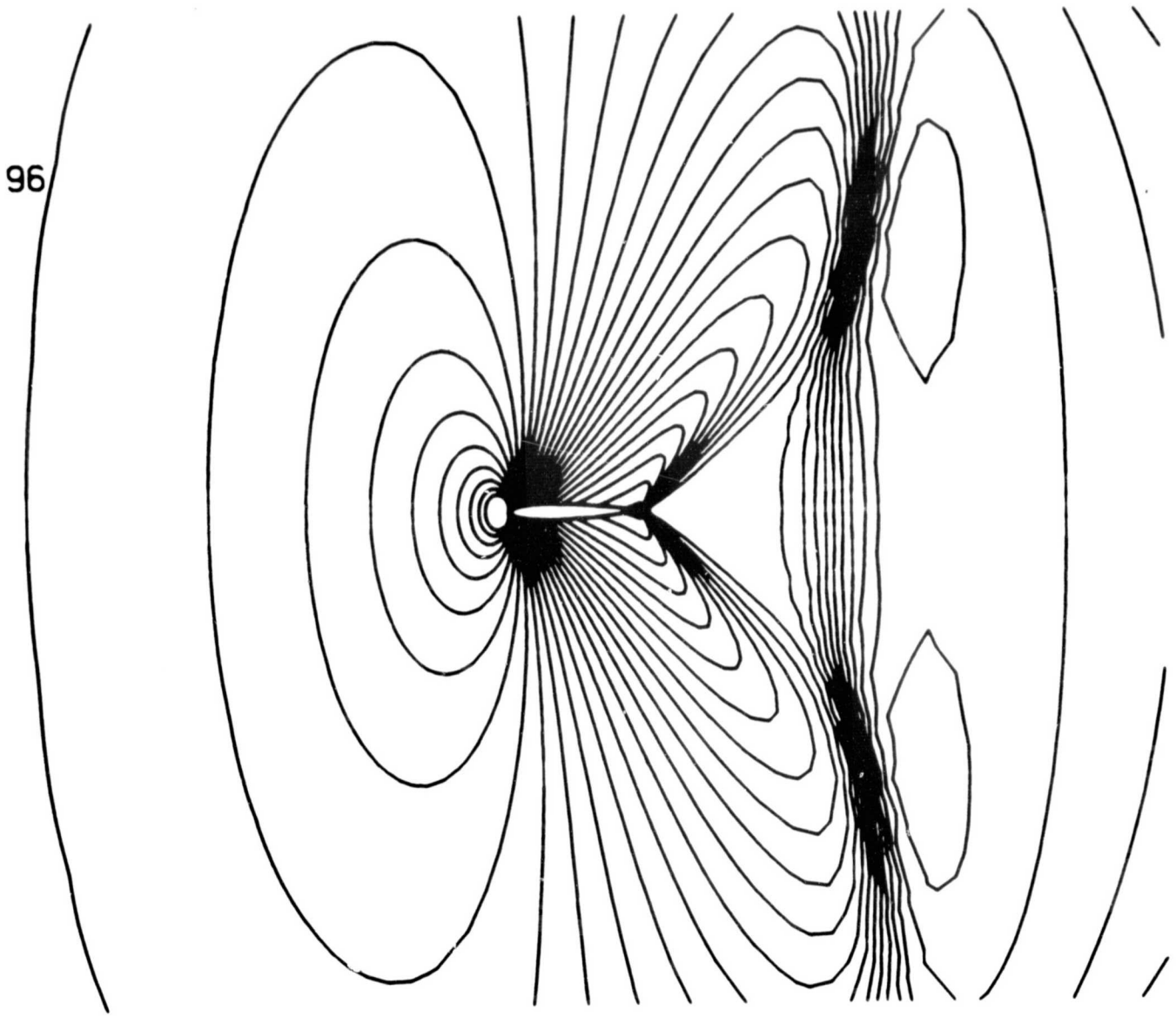

Figure 6.- Mach number contours NACA 0012 airfoil, $M_\infty = 0.98$, $\alpha = 0°$ (80 iterations).

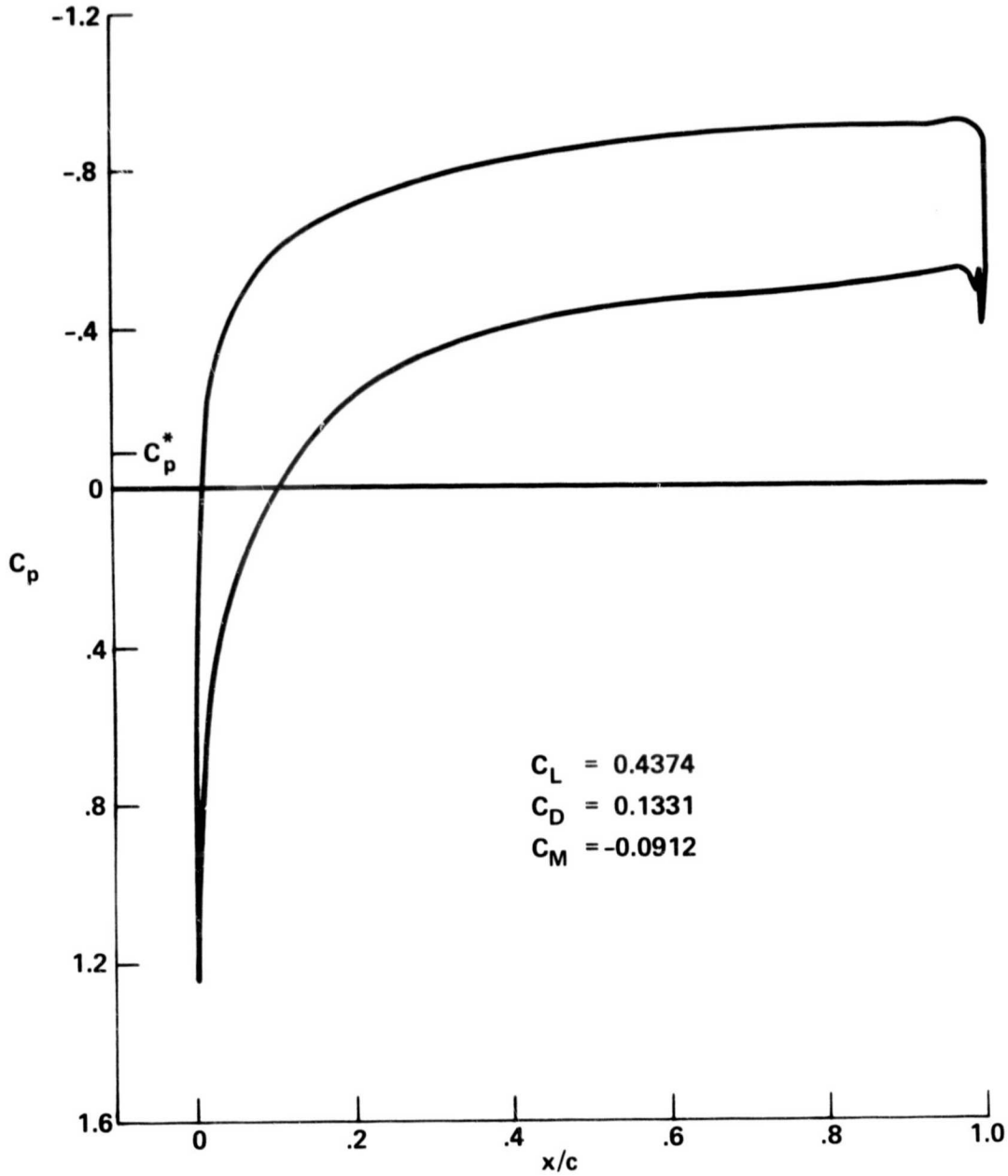

Figure 7.- Pressure coefficient distribution, NACA 0012 airfoil, $M_\infty = 0.95$, $\alpha = 4°$.

96

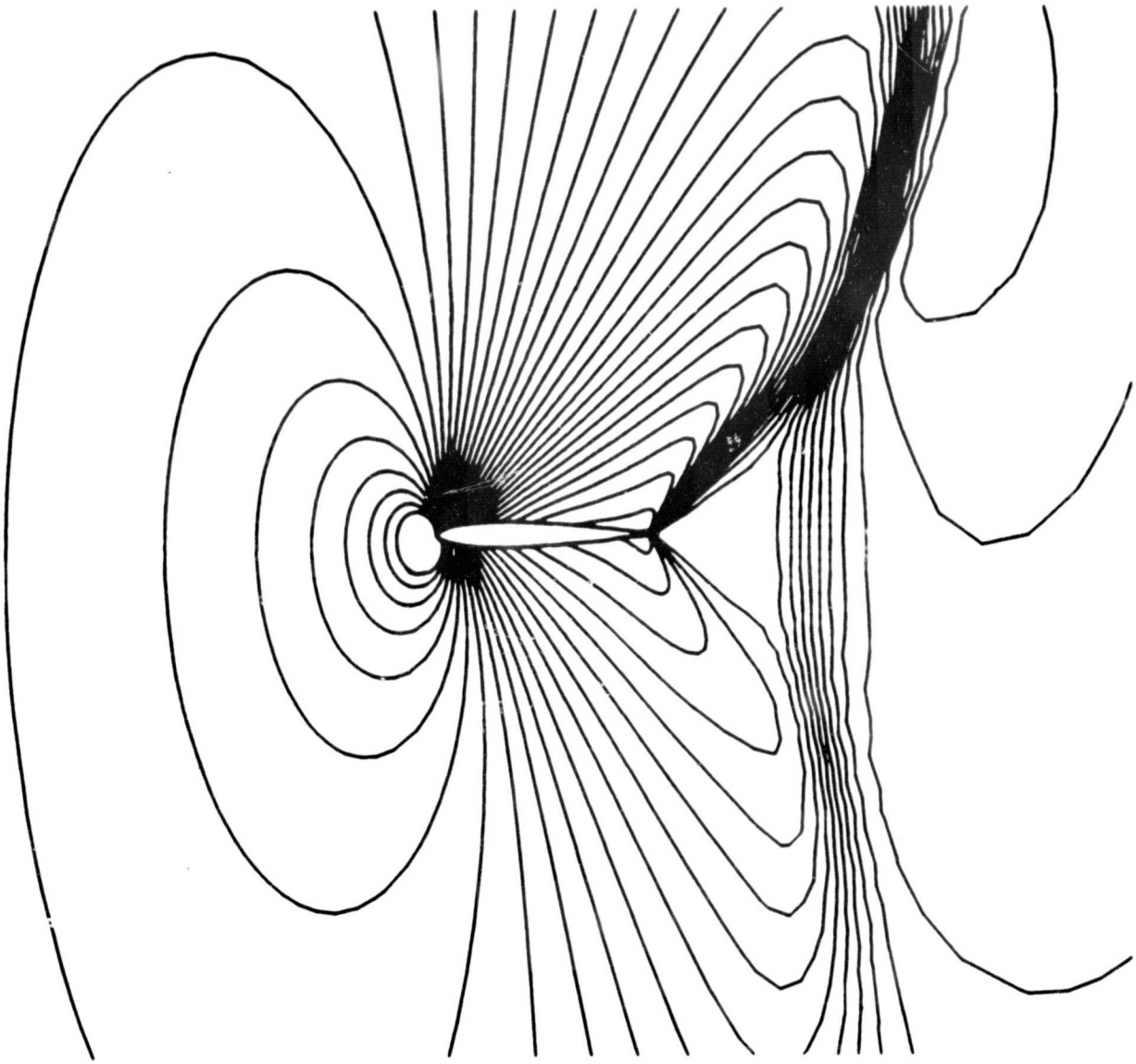

Figure 8.- Mach number contours, NACA 0012 airfoil, $M_\infty = 0.95$, $\alpha = 4°$ (96 iterations).

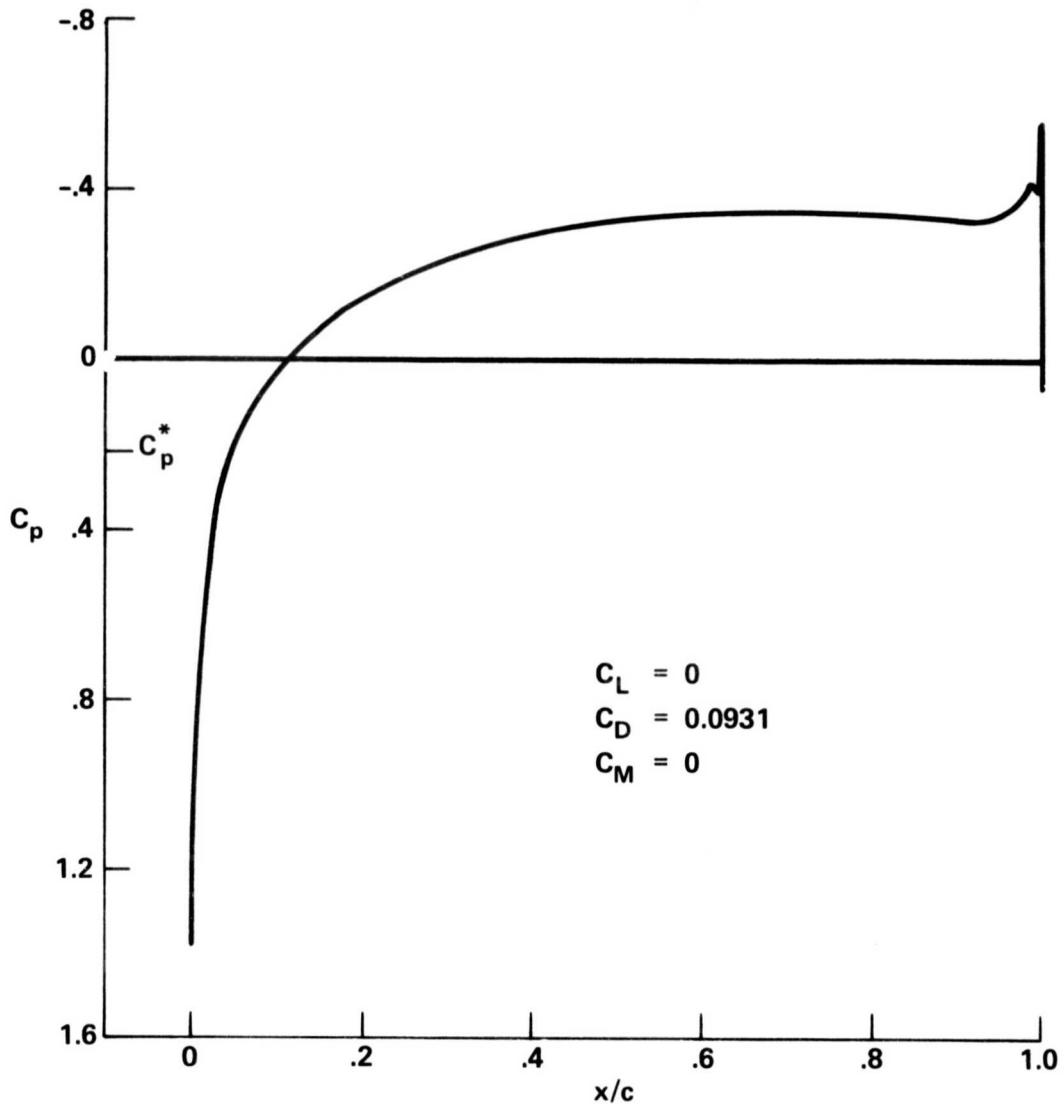

Figure 9.- Pressure coefficient distribution, NACA 0012 airfoil, $M_\infty = 1.15$, $\alpha = 0°$.

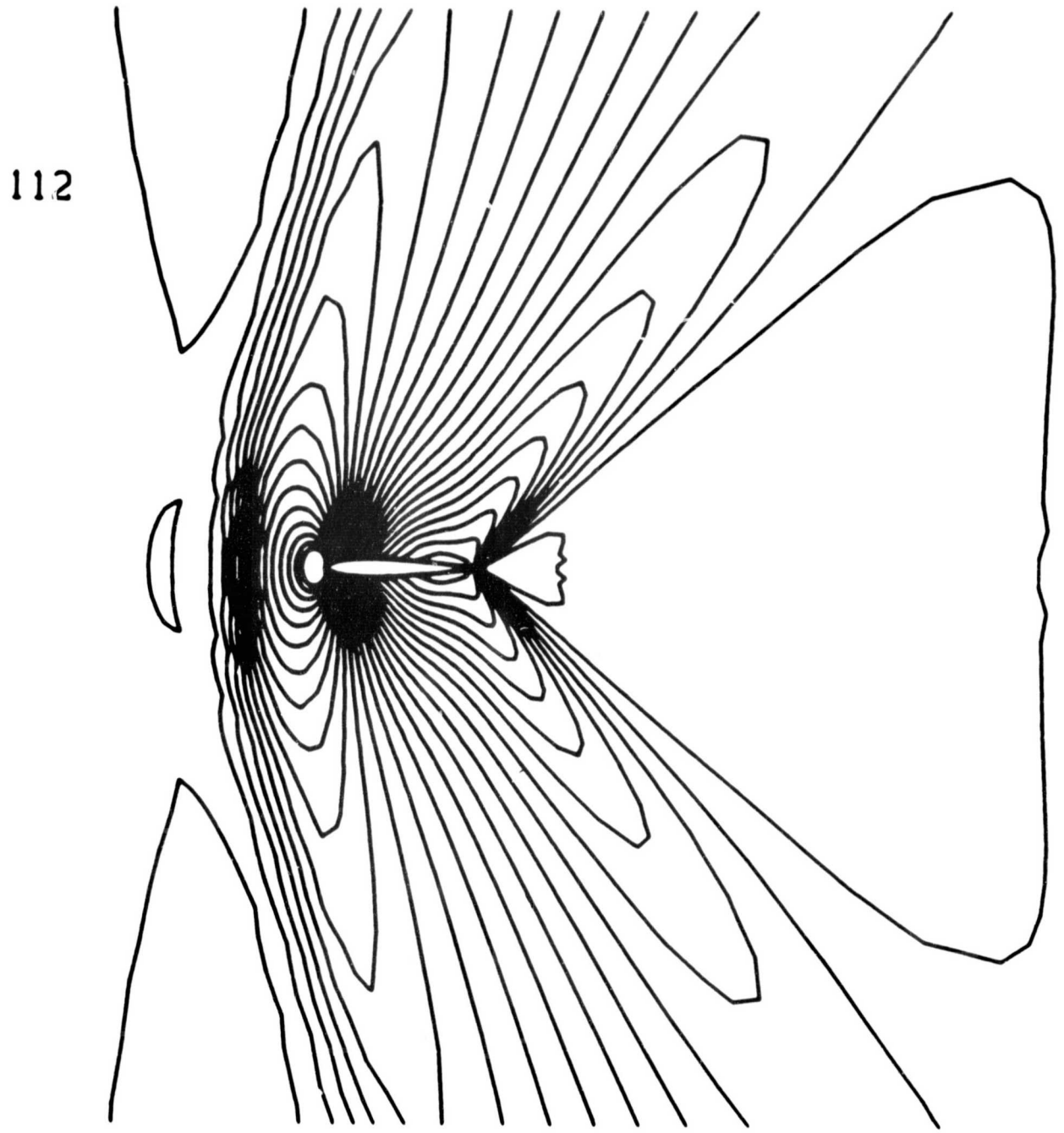

Figure 10.- Mach number contours, NACA 0012 airfoil, $M_\infty = 1.15$, $\alpha = 0°$ (128 iterations).

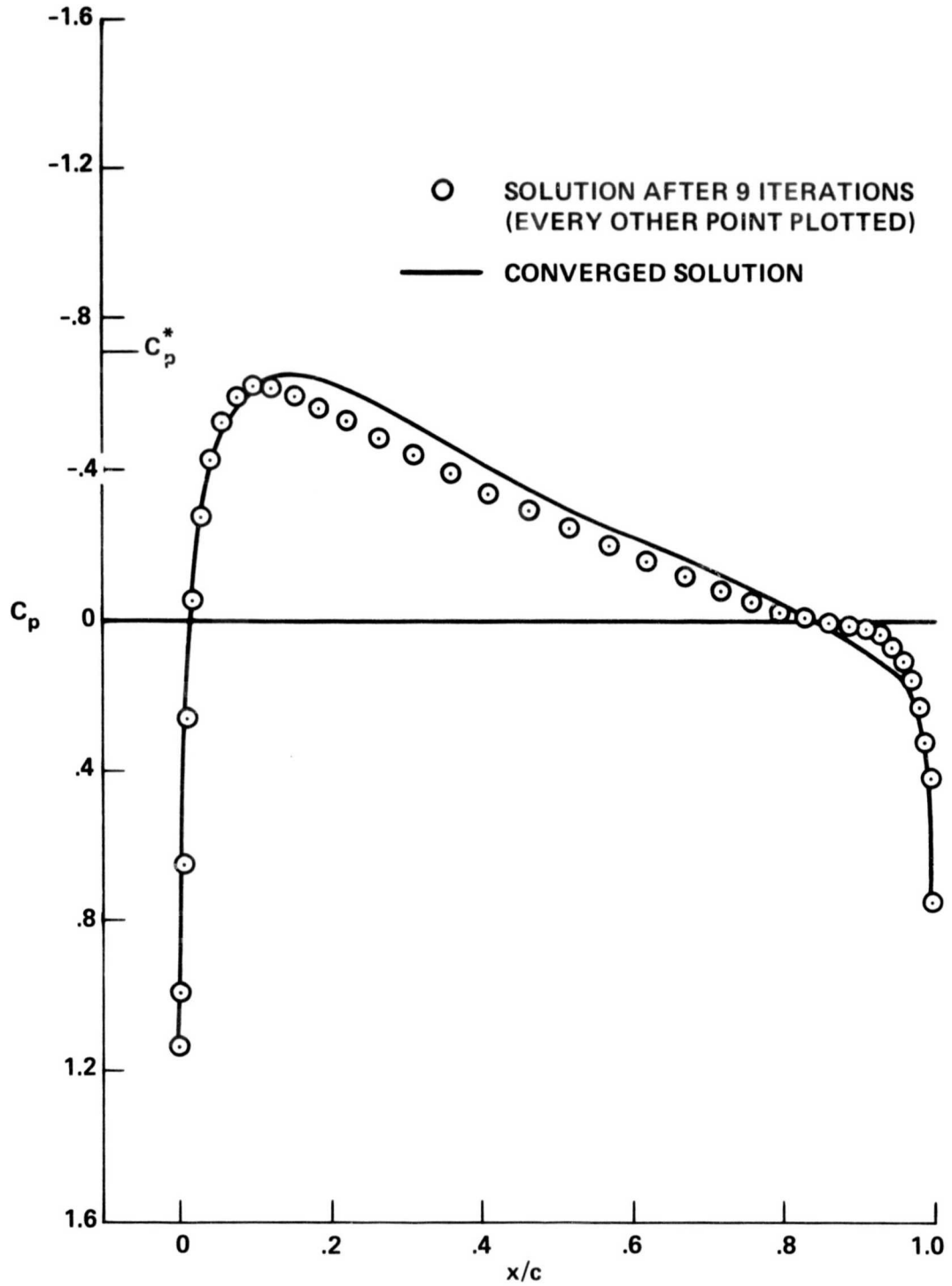

Figure 11.- Intermediate solution comparison, NACA 0012 airfoil, $M_\infty = 0.72$, $\alpha = 0°$.

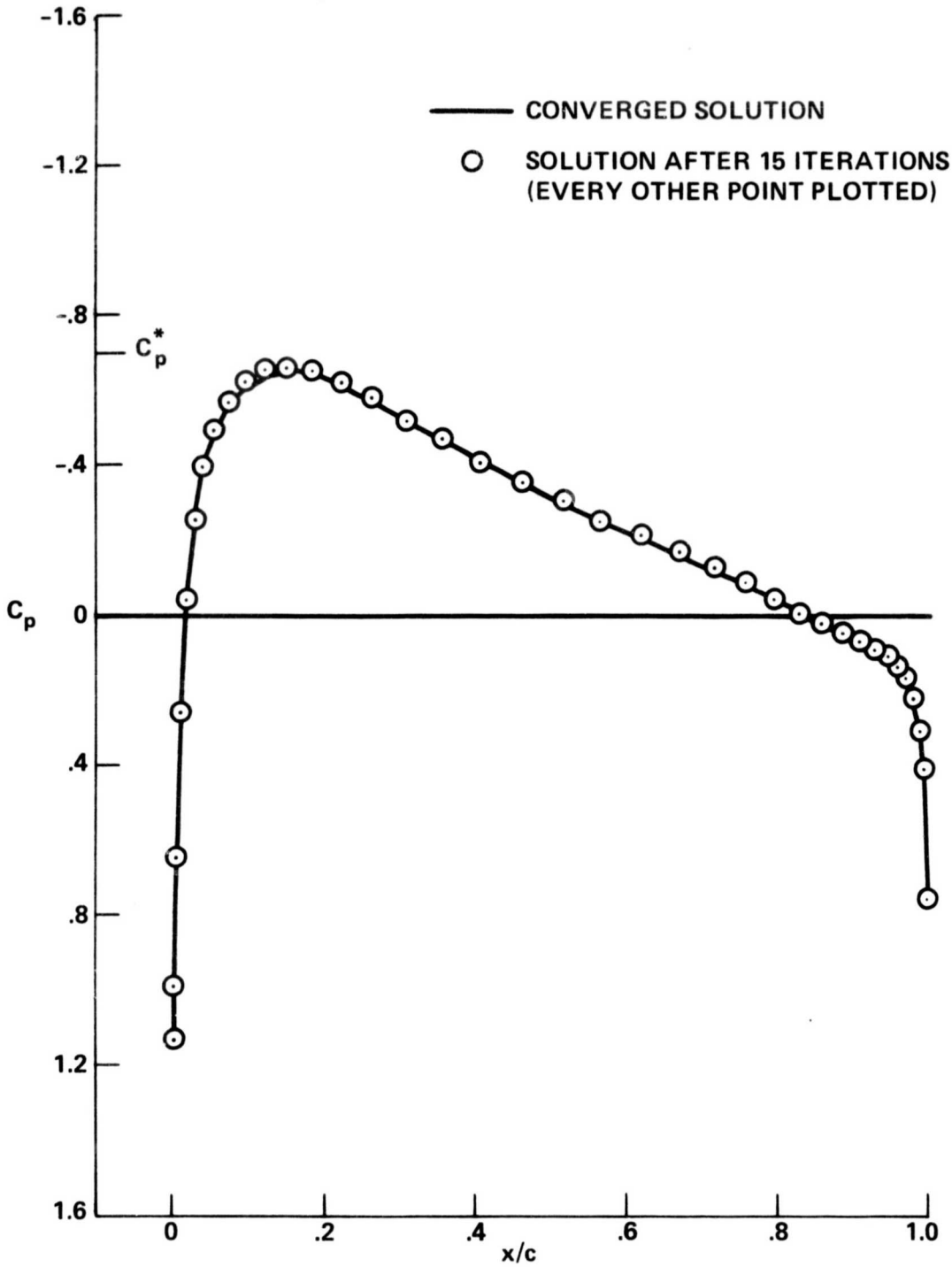

Figure 12.- Intermediate solution comparison, NACA 0012 airfoil, $M_\infty = 0.72$, $\alpha = 0°$.

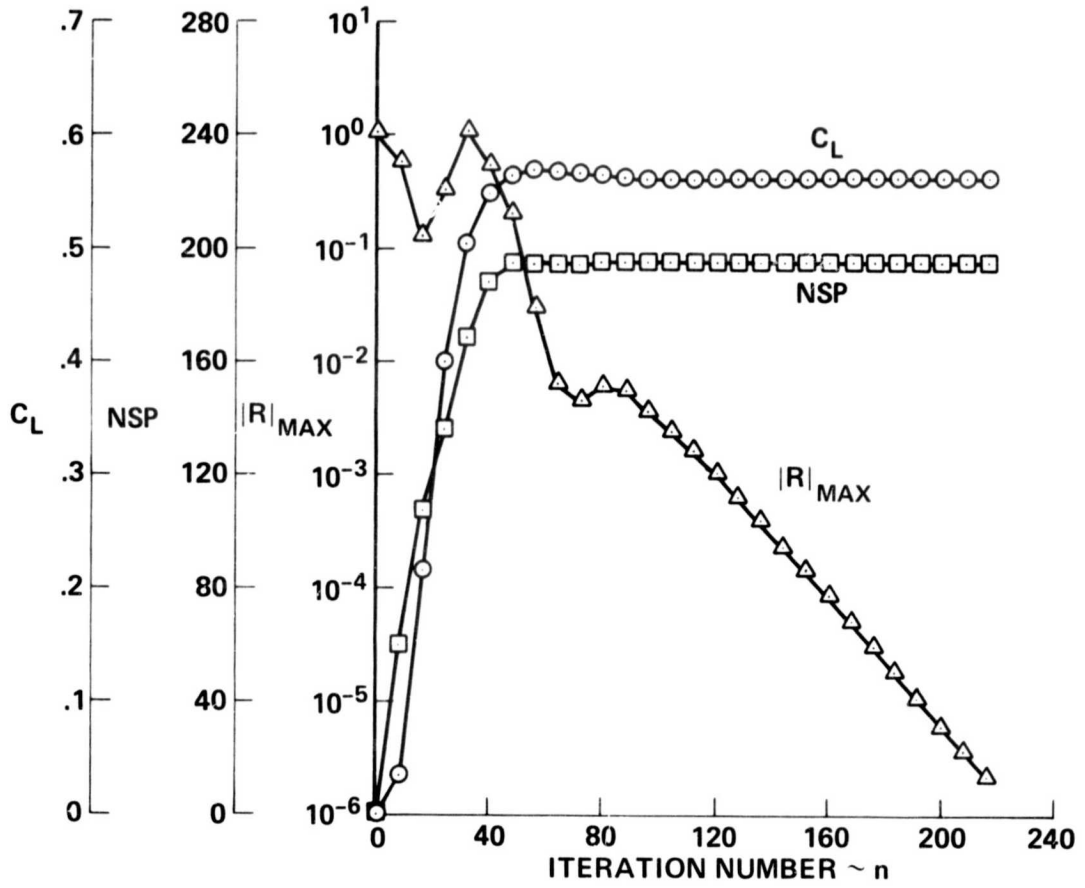

Figure 13.- Convergence history, NACA 0012 airfoil, $M_\infty = 0.75$, $\alpha = 2°$.

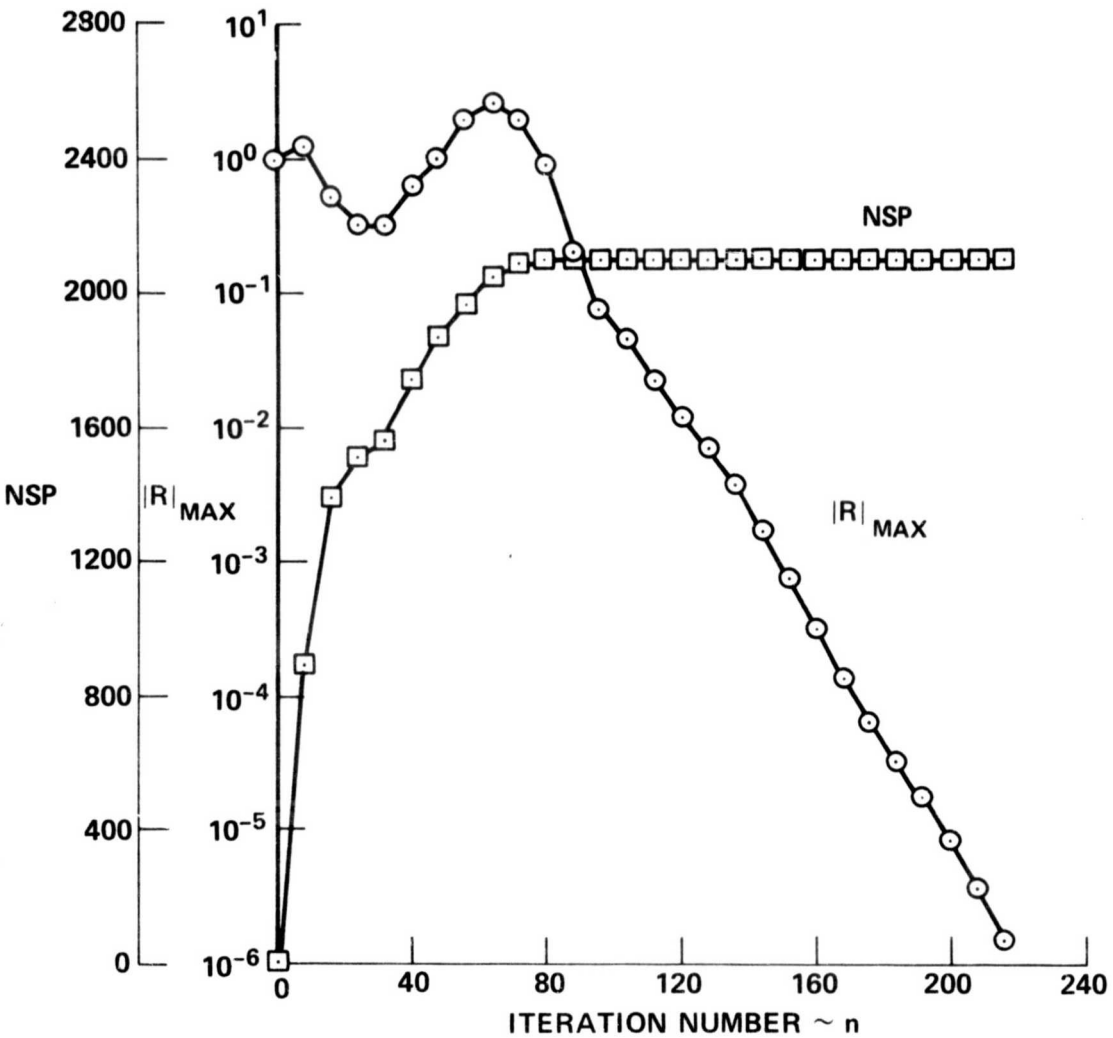

Figure 14.- Convergence history, NACA 0012 airfoil, $M_\infty = 0.98$, $\alpha = 0°$.

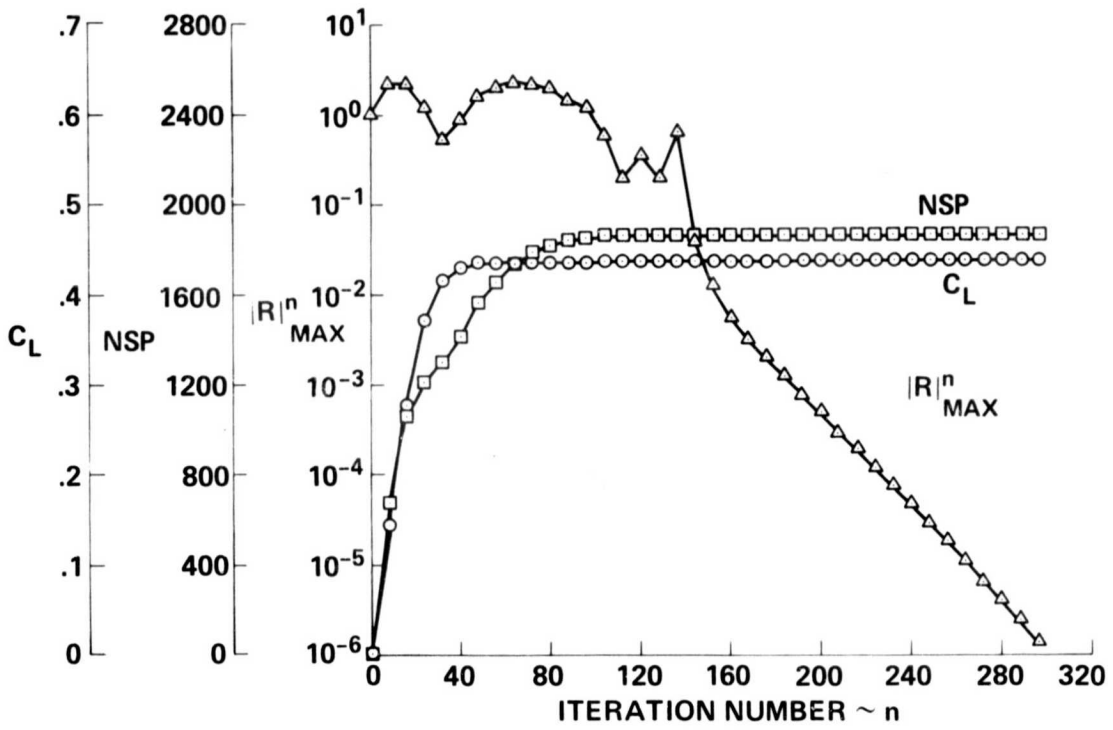

Figure 15.- Convergence history, NACA 0012 airfoil, $M_\infty = 0.95$, $\alpha = 4°$.

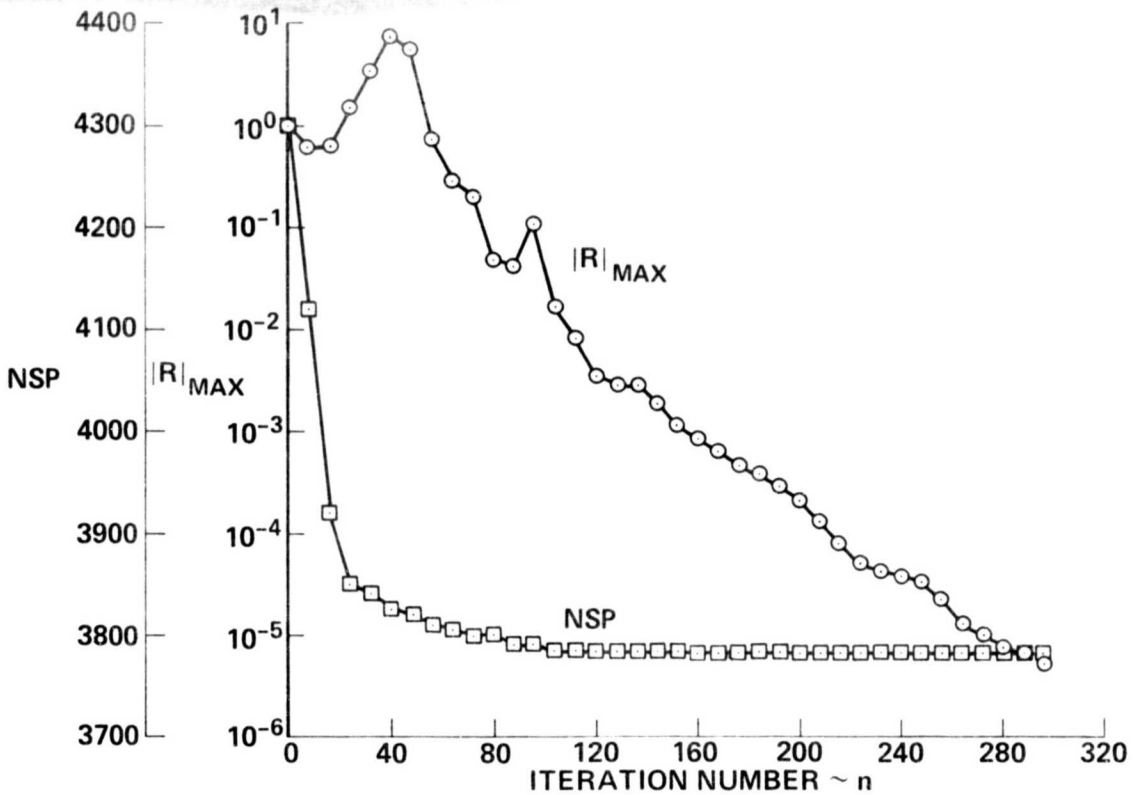

Figure 16.- Convergence history, NACA 0012 airfoil, $M_\infty = 1.15$, $\alpha = 0°$.

1. Report No. NASA TM-78570	2. Government Accession No.	3. Recipient's Catalog No.
4. Title and Subtitle AN IMPLICIT ALGORITHM FOR THE CONSERVATIVE, TRANSONIC FULL POTENTIAL EQUATION WITH EFFECTIVE ROTATED DIFFERENCING		5. Report Date 6. Performing Organization Code
7. Author(s) Terry L. Holst* and John Albert**		8. Performing Organization Report No. A-7768
9. Performing Organization Name and Address *NASA-Ames Research Center, Moffett Field, Calif. 94035 **University of Santa Clara, Santa Clara, Calif.		10. Work Unit No. 505-06-11 11. Contract or Grant No.
12. Sponsoring Agency Name and Address National Aeronautics and Space Administration Washington, D.C. 20546		13. Type of Report and Period Covered Technical Memorandum 14. Sponsoring Agency Code

15. Supplementary Notes

16. Abstract

A new differencing scheme for the conservative full potential equation which effectively simulates rotated differencing is presented. The scheme is implemented by an appropriate upwind bias of the density coefficient along both coordinate directions. A fast, fully implicit, approximate factorization iteration scheme is then used to solve the resulting difference equations. Solutions for a number of traditionally difficult transonic airfoil test cases are presented.

17. Key Words (Suggested by Author(s))	18. Distribution Statement
Transonic flow Numerical methods	Unlimited STAR Category - 02

19. Security Classif. (of this report)	20. Security Classif. (of this page)	21. No. of Pages	22. Price*
Unclassified	Unclassified	35	$4.00

*For sale by the National Technical Information Service, Springfield, Virginia 22161